

Broadband enhancement of single photon emission and polarization dependent coupling in silicon nitride waveguides

Suzanne Bisschop,^{1,2,3} Antoine Guille,^{1,3} Dries Van Thourhout,^{2,3}
Zeger Hens,^{1,3} and Edouard Brainis^{1,3,*}

¹Physics and Chemistry of Nanostructures, Ghent University, Krijgslaan 281-S3, 9000 Ghent, Belgium

²Photonics Research Group, INTEC Department, Ghent University-IMEC, Sint-Pietersnieuwstraat 41, 9000 Ghent, Belgium

³Center for Nano and Biophotonics (NB Photonics), Ghent University, B-9000 Ghent, Belgium

*Edouard.Brainis@ugent.be

Abstract: Single-photon (SP) sources are important for a number of optical quantum information processing applications. We study the possibility to integrate triggered solid-state SP emitters directly on a photonic chip. A major challenge consists in efficiently extracting their emission into a single guided mode. Using 3D finite-difference time-domain simulations, we investigate the SP emission from dipole-like nanometer-sized inclusions embedded into different silicon nitride (SiN_x) photonic nanowire waveguide designs. We elucidate the effect of the geometry on the emission lifetime and the polarization of the emitted SP. The results show that highly efficient and polarized SP sources can be realized using suspended SiN_x slot-waveguides. Combining this with the well-established CMOS-compatible processing technology, fully integrated and complex optical circuits for quantum optics experiments can be developed.

© 2015 Optical Society of America

OCIS codes: (270.0270) Quantum optics; (230.3120) Integrated optics devices; (220.0220) Optical design and fabrication; (130.2790) Guided waves; (230.6080) Sources.

References and links

1. E. Knill, R. Laflamme, and G. J. Milburn, "A scheme for efficient quantum computation with linear optics," *Nature* **409**, 46–52 (2001).
2. M. Varnava, D. E. Browne, and T. Rudolph, "How good must single photon sources and detectors be for efficient linear optical quantum computation?" *Phys. Rev. Lett.* **100**, 060502 (2008).
3. T. D. Ladd, F. Jelezko, R. Laflamme, Y. Nakamura, C. Monroe, and J. L. O'Brien, "Quantum computers," *Nature* **464**, 45–53 (2010).
4. N. Gisin, G. Ribordy, W. Tittel, and H. Zbinden, "Quantum cryptography," *Rev. Mod. Phys.* **74**, 145–195 (2002).
5. V. Scarani, H. Bechmann-Pasquinucci, N. J. Cerf, M. Dušek, N. Lütkenhaus, and M. Peev, "The security of practical quantum key distribution," *Rev. Mod. Phys.* **81**, 1301–1350 (2009).
6. M. Rau, T. Heindel, S. Unsleber, T. Braun, J. Fischer, S. Frick, S. Nauerth, C. Schneider, G. Vest, S. Reitzenstein, M. Kamp, A. Forchel, S. Höfling, and H. Weinfurter, "Free space quantum key distribution over 500 meters using electrically driven quantum dot single-photon sources: a proof of principle experiment," *New J. Phys.* **16**, 043003 (2014).
7. J. F. Dynes, Z. L. Yuan, A. W. Sharpe, and A. J. Shields, "A high speed, postprocessing free, quantum random number generator," *Appl. Phys. Lett.* **93**, 031109 (2008).

8. C. H. Bennett, F. Bessette, G. Brassard, L. Salvail, and J. Smolin, "Experimental quantum cryptography," *J. Cryptology* **5**, 3–28 (1992).
9. S. Takeuchi, "Experimental demonstration of a three-qubit quantum computation algorithm using a single photon and linear optics," *Phys. Rev. B* **62**, 032301 (2000).
10. E. Brainis, L.-P. Lamoureux, N. J. Cerf, P. Emplit, M. Haelterman, and S. Massar, "Fiber-optics implementation of the Deutsch-Jozsa and Bernstein-Vazirani quantum algorithms with three qubits," *Phys. Rev. Lett.* **90**, 157902 (2003).
11. L.-P. Lamoureux, E. Brainis, D. Amans, J. Barrett, and S. Massar, "Provably secure experimental quantum bit-string generation," *Phys. Rev. Lett.* **94**, 050503 (2005).
12. L.-P. Lamoureux, E. Brainis, N. J. Cerf, P. Emplit, M. Haelterman, and S. Massar, "Experimental error filtration for quantum communication over highly noisy channels," *Phys. Rev. Lett.* **94**, 230501 (2005).
13. A. Crespi, R. Osellame, R. Ramponi, D. J. Brod, E. F. Galvão, N. Spagnolo, C. Vitelli, E. Maiorino, P. Mataloni, and F. Sciarrino, "Integrated multimode interferometers with arbitrary designs for photonic boson sampling," *Nat. Photonics* **7**, 545–549 (2013).
14. A. Politi, M. J. Cryan, J. G. Rarity, S. Yu, and J. L. O'Brien, "Silica-on-silicon waveguide quantum circuits," *Science* **320**, 646–649 (2008).
15. J. B. Spring, B. J. Metcalf, P. C. Humphreys, W.S. Kolthammer, X.-M. Jin, M. Barbieri, A. Datta, N. Thomas-Peter, N.K. Langford, D. Kundys, J. C. Gates, B. J. Smith, P. G. R. Smith, and I. A. Walmsley, "Boson sampling on a photonic chip," *Science* **339**, 798–801 (2013).
16. N. Spagnolo, C. Vitelli, M. Bentivegna, D. J. Brod, A. Crespi, F. Flamini, S. Giacomini, G. Milani, R. Ramponi, P. Mataloni, R. Osellame, E. F. Galvão, and F. Sciarrino, "Experimental validation of photonic boson sampling," *Nat. Photonics* **8**, 615–620 (2014).
17. J. Claudon, J. Bleuse, N. S. Malik, M. Bazin, P. Jaffrennou, N. Gregersen, C. Sauvan, P. Lalanne, and J.-M. Gérard, "A highly efficient single-photon source based on a quantum dot in a photonic nanowire," *Nat. Photonics* **4**, 174–177 (2010).
18. N. Gregersen, T. R. Nielsen, J. Mørk, J. Claudon, and J.-M. Gérard, "Designs for high-efficiency electrically pumped photonic nanowire single-photon sources," *Opt. Express* **18**, 21204–21218 (2010).
19. M. E. Reimer, G. Bulgarini, N. Akopian, M. Hocevar, M. B. Bavinck, M. A. Verheijen, E.P.A.M. Bakkers, L. P. Kouwenhoven, and V. Zwiller, "Bright single-photon sources in bottom-up tailored nanowires," *Nat. Commun.* **3**, 737 (2012).
20. X. Brokmann, G. Messin, P. Desbiolles, E. Giacobino, M. Dahan, and J. P. Hermier, "Colloidal CdSe/ZnS quantum dots as single-photon sources," *New J. Phys.* **6**, 99 (2004).
21. Y. Chen, J. Vela, H. Htoon, J. L. Casson, D. J. Werder, D. A. Bussian, V. I. Klimov, and J. A. Hollingsworth, "'giant' multishell CdSe nanocrystal quantum dots with suppressed blinking," *J. Am. Chem. Soc.* **130**, 5026–5027 (2008).
22. B. Mahler, P. Spinicelli, S. Buil, X. Quelin, J.-P. Hermier, and B. Dubertret, "Towards non-blinking colloidal quantum dots," *Nat. Mater.* **7**, 659–664 (2008).
23. F. Pisanello, L. Martiradonna, G. Leménager, P. Spinicelli, A. Fiore, L. Manna, J.-P. Hermier, R. Cingolani, E. Giacobino, M. De Vittorio, and A. Bramati, "Room temperature-dipolelike single photon source with a colloidal dot-in-rod," *Appl. Phys. Lett.* **96**, 033101 (2010).
24. A. Beveratos, R. Brouri, T. Gacoin, J.-P. Poizat, and P. Grangier, "Nonclassical radiation from diamond nanocrystals," *Phys. Rev. B* **64**, 061802 (2001).
25. Y. Shen, T. M. Sweeney, and H. Wang, "Zero-phonon linewidth of single nitrogen vacancy centers in diamond nanocrystals," *Phys. Rev. C* **77**, 033201 (2008).
26. R. Kolesov, K. Xia, R. Reuter, R. Stöhr, A. Zappe, J. Meijer, P. R. Hemmer, and J. Wrachtrup, "Optical detection of a single rare-earth ion in a crystal," *Nat. Commun.* **3**, 1029 (2012).
27. B. De Geyter, K. Komorowska, E. Brainis, P. Emplit, P. Geiregat, A. Hassinen, Z. Hens, and D. Van Thourhout, "From fabrication to mode mapping in silicon nitride microdisks with embedded colloidal quantum dots," *Appl. Phys. Lett.* **101**, 161101 (2012).
28. Q. Xu, V. R. Almeida, R. R. Panepucci, and M. Lipson, "Experimental demonstration of guiding and confining light in nanometer-size low-refractive-index material," *Opt. Lett.* **29**, 1626–1628 (2004).
29. M. Galli, D. Gerace, A. Politi, M. Liscidini, M. Patrini, L. C. Andreani, A. Canino, M. Miritello, R. L. Savio, A. Irrera, and F. Priolo, "Direct evidence of light confinement and emission enhancement in active silicon-on-insulator slot waveguides," *Appl. Phys. Lett.* **89**, 241114 (2006).
30. Y. C. Chul, R. M. Briggs, H. A. Atwater, and M. L. Brongersma, "Broadband enhancement of light emission in silicon slot waveguides," *Opt. Express* **17**, 7479–7490 (2009).
31. J.-M. Gérard and B. Gayral, "Strong Purcell effect for InAs quantum boxes in three-dimensional solid-state microcavities," *J. Lightwave Technol.* **17**, 2089–2095 (1999).

1. Introduction

Single-photon (SP) sources are important for a number of optical quantum information processing applications such as quantum computing [1–3], quantum cryptography [4–6], and random number generation [7]. In these applications, the photon wave function is processed by performing operations such as polarization rotations, phase shifts and path splitting/recombination in order to en- or decode information. In early demonstrations of quantum computing and quantum communication protocols, these operations were usually performed with table-top optical components [8, 9], and later with fibre optics elements [10–12]. These approaches offer high flexibility but suffer from thermal and mechanical instabilities that hinder their scalability. Complex optical circuits are best realized using integrated photonic devices on a micro-chip. Many recent experiments successfully validated this approach by performing quantum optics experiments with photons propagating in integrated photonic circuits [13–16].

In this work, we study the possibility to integrate triggered *solid-state* SP emitters *directly* on a photonic chip. A major challenge consists in efficiently extracting their emission into a single guided mode. This is seen by many as a stumbling block precluding their usage in practical implementations. In 2010, a record photon extraction efficiency of 72% was first demonstrated by embedding the SP emitter into a tapered photonic nanowire [17–19]. Following this approach, we consider different source designs in which the SP emitter is embedded into a photonic nanowire *waveguide*. This contrasts with the traditional approach consisting in placing the emitter in a high Q/V cavity, a method that is only efficient for very narrowband emitters such as epitaxially grown quantum dots at cryogenic temperatures. A good polarization control is key to most applications, including linear quantum computing and quantum cryptography. As shown in this work, efficient, directive, and broadband SP sources with well defined polarization states can be engineered.

We specifically investigate photonic chips made of silicon nitride (SiN_x) devices. SiN_x is an amorphous material that has a larger refractive index than silica ($n = 2$) and is highly transparent in both visible and near-infrared ranges. In addition, SiN_x devices and circuits can be realized on a silicon-on-insulator chip using standard CMOS compatible processing technologies. This technology is suitable for developing a universal platform for quantum optics and quantum information processing applications in conjunction with many common solid-state emitters. It offers the possibility to embed alien solid-state inclusions acting as SP emitters directly inside the SiN_x host. Such inclusions can be colloidal quantum dots [20–23], nanoparticles containing a single color centre [24, 25], or nanoparticles doped with a single ion [26]. This approach offers a very flexible route to future on-chip quantum optics experiments by separating the engineering of the emitter from the engineering of the photonic circuit itself. In addition this approach would also be scalable since it allows many integrated SP sources and optical circuits to operate in parallel. In this prospect, colloidal quantum dots are of primary interest for proof-of-principle demonstrations because of their ability to emit single photons with a quantum yield as high as 80% at room temperatures [20–23] and the fact that their embedding in SiN_x photonic structures has been recently achieved [27].

We investigate the SP emission from dipole-like nanometer-sized inclusions embedded in four types of SiN_x waveguiding structures as represented in Fig. 1. The first and simplest structure is a strip SiN_x waveguide on the top of a silicon oxide (SiO_x) substrate (Fig. 1(a)). A more elaborated design giving better performance consists in a slot waveguide in which a SiO_x layer is sandwiched between a lower and upper SiN_x layer (Fig. 1(c)). Using wet etching the substrate can be removed to create suspended strip and slot waveguides such as those represented in Figs. 1(b) and 1(c), respectively. In each case, the SP emitter is positioned at the center of the structure. They are assumed to be effectively degenerate two-level systems with no preferential dipole moment orientation. Several experiments and theoretical works investigated light emis-

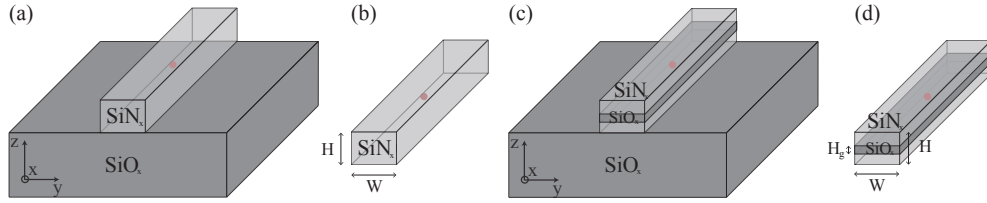


Fig. 1. Layout of the simulated structures. (a) Silicon nitride (SiN_x) strip waveguide on top of silicon oxide (SiO_x) substrate. (b) suspended SiN_x strip waveguide. (c) SiN_x slot waveguide on top of SiO_x substrate with SiO_x slot. (d) suspended SiN_x slot waveguide with SiO_x slot. The dipole is located at the center of the waveguide (red dot).

sion in such silicon stripe and slot structures [28–30]. Here, we extend this work to realistic 3D SiN_x structures. More importantly, we elucidate the effect of the geometry on the emission lifetime and the polarization of the emitted single photons.

2. Light emission from randomly polarized dipoles

As is well known, both the spontaneous emission rate and the radiation pattern of the light emitted by a quantum dipole transition depend on the environment into which the light is emitted. The spontaneous emission rate from a non degenerate two-level dipole transition is given by Fermi's Golden Rule [31]:

$$\Gamma = \frac{2\pi}{\hbar^2} \sum_{\sigma} |\mathbf{d} \cdot \mathbf{E}_{\sigma}(\mathbf{r}_e)|^2 \rho_{\sigma}(\omega) \quad (1)$$

where ω and \mathbf{d} are the Bohr frequency and the dipole moment matrix element of the transition. The sum runs over all the optical modes (labelled by the index σ) that are coupled to the emitter. Here, $\rho_{\sigma}(\omega)$ stands for the mode density at frequency of the transition and $\mathbf{E}_{\sigma}(\mathbf{r}_e) = \sqrt{\frac{\hbar\omega}{2\epsilon_0}} \mathbf{v}_{\sigma}(\mathbf{r}_e)$ for the modal vacuum field amplitude. The modal function $\mathbf{v}_{\sigma}(\mathbf{r}_e)$ is normalized such that $\int n^2(\mathbf{r}) |\mathbf{v}(\mathbf{r})|^2 d^3r = 1$, where $n(\mathbf{r})$ is the index of refraction of the environment. From Eq. (1), we see that two main factors influence the spontaneous emission rate: (i) the modal field intensities at the position of the emitter and (ii) the spectral densities of the modes at the frequency of the emitting transition. The modes to take into account include guided modes as well as radiated modes. With a careful design of the waveguide one can modify both these factors by changing the number of guided modes (with specific polarization; TE or TM) and their mode profiles. The resulting spontaneous emission rate can be quite different from the rate Γ_0 that one would observe if the emitter was embedded in a homogeneous medium of index $n(\mathbf{r}_e)$. The enhancement (or inhibition) of the spontaneous emission rate due to the structuring of the photonic environment of the emitter is expressed by the *Purcell factor*

$$F = \frac{\Gamma}{\Gamma_0} \quad (2)$$

In the case of a randomly polarized SP emitter, the orientation of the dipole moment \mathbf{d} is random. Each orientation direction $i \in \{x, y, z\}$ can be seen as an independent de-excitation channel for the emitter. Therefore the total spontaneous emission rate is the sum of the spontaneous emission rates Γ_i corresponding to each possible orientation: $\Gamma = \sum_i \Gamma_i$. In a nanostructured environment such as a waveguide, the rates Γ_i will generally differ from each other and so will

the Purcell factors $F_i = \Gamma_i/\Gamma_0$ associated to each possible vibration direction. The spontaneous emission enhancement is measured by the Purcell factor: $F = \Gamma/\Gamma_0 = \sum_i F_i$. When a single photon is emitted as a result of a de-excitation process, the probability that it is emitted by a dipole oscillating in the i -direction is

$$p_i = \frac{\Gamma_i}{\Gamma} = \frac{F_i}{F} \quad (3)$$

Waveguides can be engineered such that a dipole oscillating in a specific direction has a much larger Purcell factor than a dipole oscillating in any other two directions. In such a case, the photonic environment would turn an intrinsically unpolarized emitter into a polarized one, one with a p_i which is much larger than the p_i for the other directions.

To make an efficient directional SP source, the light from the SP emitter must mainly couple to the *guided* modes of the waveguide. Since photon emission into the guided and radiated modes can be seen as independent de-excitation channels, each spontaneous emission rate $\Gamma_i = \Gamma_i^g + \Gamma_i^r$ can be further split into an emission rate into the guided modes (Γ_i^g) and an emission rate into the radiated modes (Γ_i^r). The fraction of light that is emitted by an i -polarized dipole into the guided modes of the waveguiding structure, is equal to $f_i = \Gamma_i^g/\Gamma_i$. For a randomly polarized SP emitter, the probability that a photon is emitted into the guided modes is given by the coupling efficiency

$$\beta = \sum_i p_i f_i = \frac{1}{\Gamma} \sum_i \Gamma_i^g \quad (4)$$

The fraction of the guided light originating from an i -polarized oscillating dipole is given by the factor

$$\beta_i = p_i f_i = \frac{\Gamma_i^g}{\Gamma} \quad (5)$$

Hence, an efficient, directional and polarized SP source requires that one of the β_i -factors, either β_y or β_z , is as close as possible to one (see coordinate system in Fig. 1).

3. Results and discussion

Light emission from a SP emitting inclusion embedded in the four photonic structures represented in Fig. 1 has been investigated by performing 3D finite-difference time-domain (FDTD) simulations. In all simulations the emitter is located at the center of the waveguide and is emitting at a wavelength of 650 nm. A photon emitted in a waveguide is in a superposition of two opposite propagation directions. The waveguide coupling factors and emission rates mentioned in the text account for both propagation directions ($\pm x$). A directional emission can be obtained by placing a reflector at one end of the waveguide.

3.1. Strip waveguides

Strip waveguides are simple to design and to fabricate using standard lithographic techniques. In the case depicted in Fig. 1(a), the strip waveguide lies on a thick silicon oxide layer (refractive index $n = 1.46$) on a silicon chip. The case in Fig. 1(b) corresponds to an under-etched waveguide: the silicon oxide layer under the waveguide has been chemically removed and the waveguide is suspended above the silicon chip. Both cases were simulated for different values of the waveguide width (W) and height (H) (see Fig. 1).

Figure 2(a) displays the fraction of the light radiated by a oscillating dipole which is effectively coupled to guided modes. The coupled fraction f_y (f_z) radiated by a horizontally (vertically) oscillating dipole is plotted with dashed (plain) lines. A dipole oscillating in the longitudinal (x) direction does not couple efficiently to the waveguide ($f_x < 0.028$ in all cases).

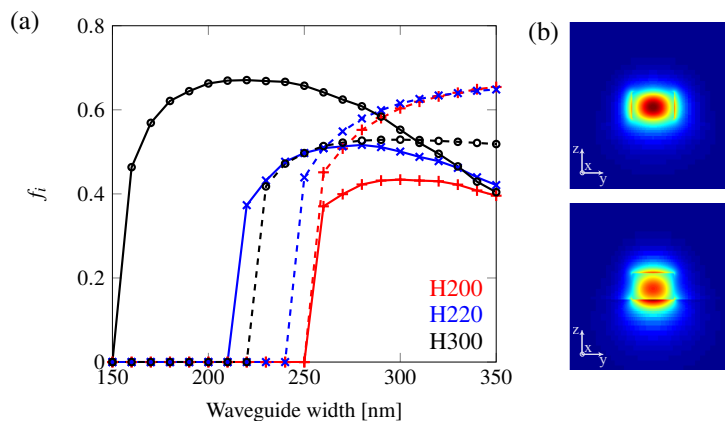


Fig. 2. Strip SiN_x waveguide on substrate: a) fraction of light radiated by a y-oscillating dipole (f_y , dashed line) and by a z-oscillating dipole (f_z , plain line) that is coupled to the guided modes as a function of the waveguide width W for three different waveguide heights $H = 200$ nm (red), 220 nm (blue), and 300 nm (black). b) Mode profiles of the two guided modes for a waveguide with $H = 220$ nm and $W = 350$ nm. Top: fundamental TE mode. Bottom: fundamental TM mode.

Three waveguide heights are considered: $H = 200$ nm (red curves), 220 nm (blue curves), and 300 nm (black curves). For each value of H , f_y and f_z are plotted as a function of the width W , ranging between 150 and 350 nm. In this parameter range, the waveguide can only support one TM mode and/or one TE mode. A vertically oscillating dipole couples mainly to the TM mode while a horizontally oscillating dipole couples mainly to the TE mode. When the width is swept from lower to higher values, the TM mode appears first. The mode profiles for a waveguide with $H = 220$ nm and $W = 350$ nm are shown in Fig. 2(b). Figure 2(a) shows that the TM (TE) is supported from $W = 160$ nm ($W = 230$ nm) in waveguides with $H = 300$ nm, and from larger widths in the case of thinner waveguides. f_y and f_z on the order of 50% and 65% respectively are achievable in 300 nm thick waveguides.

FDTD simulations were performed to calculate the radiation damping rates for dipoles oscillating in the three i -directions. The deduced Purcell factors F_i are found to be almost independent of the dipole polarization direction and the resulting probabilities p_i to emit in a specific polarization range between 0.21 and 0.45 in the entire range of interest. In Fig. 3, the total coupling factor β (Fig. 3(a)) and the partial coupling factors β_y and β_z (Fig. 3(b)) are shown for the same waveguide geometries as in Fig. 2. For the taller waveguides ($H = 300$ nm), Fig. 3(a) shows that the coupling to the waveguide is only 25% in the single mode regime since only the field radiated by the z -polarization is guided. However, the collected light is perfectly polarized (TM mode). In the two-mode regime a collection efficiency of 40% can be reached at the expense of losing the control over the polarization state of the collected photon. Clearly the light collection efficiency in a strip SiN_x waveguide is not high enough to make an efficient single photon source. However, the coupling can be dramatically improved by modifying the design of the waveguide.

The simplest modification consists in underetching the strip waveguide to create a suspended structure such as the one depicted in Fig. 1(b). The underetching provides a better light confinement of the guided modes which improves the coupling to the emitter. In the range of heights and widths considered here the waveguide supports at least two modes: the fundamental TE and

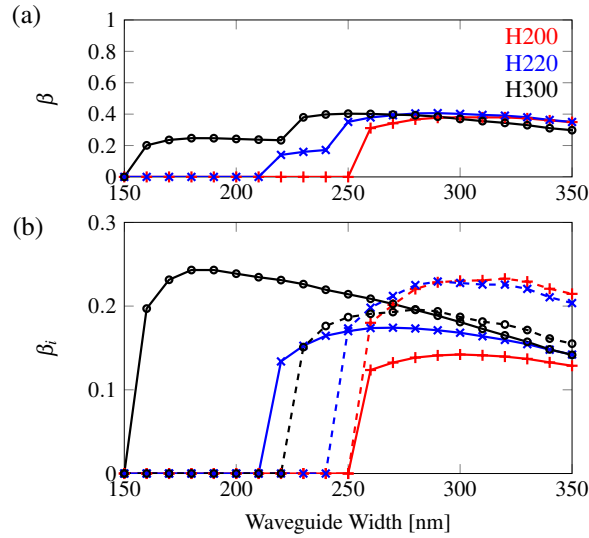


Fig. 3. Strip SiN_x waveguide on substrate: a) Total coupling factor β to the guided modes as a function of the waveguide width W for three different waveguide heights $H = 200$ nm (red), 220 nm (blue), and 300 nm (black). b) Polarization dependent coupling factors β_y (dashed line) and β_z (plain line) as a function of the waveguide width W for three different waveguide heights $H = 200$ nm (red), 220 nm (blue), and 300 nm (black).

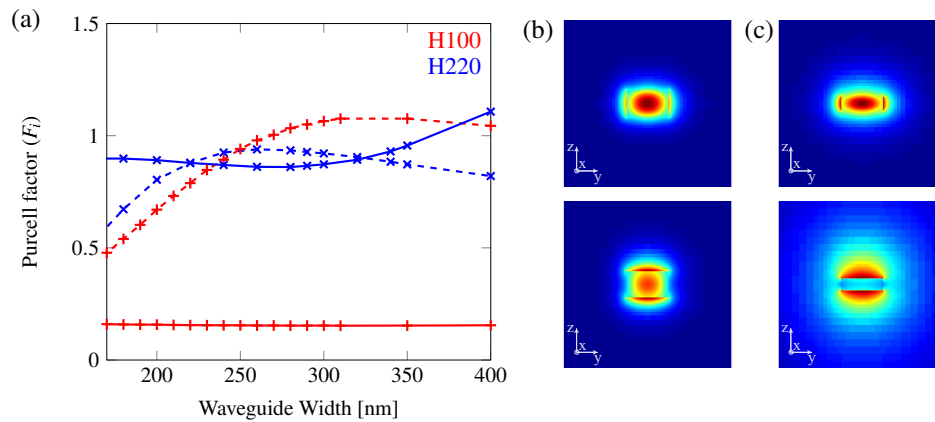


Fig. 4. Suspended SiN_x waveguide: a) Partial Purcell factor F_y (dashed line), and F_z (plain line) as a function of the waveguide width W for two waveguide heights: $H = 100$ nm (red line) and $H = 220$ nm (blue line). Mode profiles of guided fundamental TE and TM modes for a waveguide with dimensions: b) $H = 220$ nm and $W = 350$ nm, c) $H = 100$ nm and $W = 350$ nm.

the following TM mode. Fig. 4 shows that for taller waveguides ($H = 220$ nm, blue lines), the partial Purcell factors F_i range between 0.6 and 1.1. As in the case of SiN_x strip waveguides, this

does not provide sufficient polarization selectivity to force the dipole to oscillate preferentially in one specific direction, and since the suspended waveguide always supports both a TE and a TM mode (see the mode profiles in Fig. 4(b)), no polarization selectivity of the photon source can be expected in this case. In thin waveguides, the field of the TM mode is expelled from within the waveguide. This is clearly seen in Fig. 4(c) for a waveguide with $H = 100$ nm. As a consequence the radiation of a z -polarized dipole is significantly inhibited (see Eq. 1), resulting in a small $F_z < 0.16$ factor. An unpolarized emitter placed in such a thin suspended waveguide would radiate as a y -polarized dipole with a probability p_y as high as 55% and potentially lead to highly polarized guided photons if the coupling to the TE mode is strong enough.

The total coupling factor β is plotted as a function of W in Fig. 5(a) for waveguides with heights $H = 100$ nm (red line) and $H = 220$ nm (blue line). In Fig. 5(b), the corresponding partial coupling factors β_y (dashed lines) and β_z (plain lines) are displayed. The coupling factor β_x is omitted because it is negligible for $H = 100$ nm and does not exceed 14% for $H = 220$ nm. In the case of tall waveguides ($H = 220$ nm, blue line), the underetching significantly improves the coupling to guided modes, the β factor reaching values higher than 60%. This is essentially due to a better field confinement as can be seen by comparing the field profiles of Fig. 4(b) to those of Fig. 2(b). However no polarization control is achievable in this case because the geometry does not provide a sufficient Purcell enhancement/inhibition and β_y and β_z have similar values, as shown in Fig. 5(b). In the case of thin waveguides ($H = 100$ nm, red line), a β -factor of 43% can be reached. The value is lower than in the case of tall waveguides because the confinement of the TM mode is worse. However, the geometry allows for a remarkable control over the polarization of the photons coupled to the waveguide. Indeed, Fig. 5 shows that the collected light is almost completely polarized in the y -direction, e.g. $\beta_y/\beta = 95\%$ for a width $W = 310$ nm. In other words, the thin suspended waveguide geometry turns a completely unpolarized single-photon emitter into a linearly polarized single-photon source with a reasonable photon collection efficiency of 43%.

3.2. Slot waveguides

The efficiency of the photon/waveguide coupling can be enhanced by embedding the emitter into a thin SiO_x layer in the center of the SiN_x waveguide (see Figs. 1(c) and 1(d)). This kind of waveguide is called a slot-waveguide. Due to the continuity of the displacement field at any interface, this nanometer-sized slot of low index material ($n = 1.46$) in between two higher index ($n = 2$) regions results in a discontinuity of the electric field near the slot boundaries. Hence a large electric field develops in the low-index slot region for the mode which has its polarization orthogonal to the slot, in this case the TM mode (z -polarization). This improves the mode confinement and enhances the field strength at the position of the emitter, improving the coupling of the light emission into the waveguide.

To illustrate the performance enhancement provided by a thin SiO_x -slot, let us consider the case of a tall ($H > W$) SiN_x strip waveguide only supporting a single TM mode (see Figs. 2(a) and 3). Such waveguides allows for the emission of perfectly polarized guided single-photons. Without a slot, the coupling efficiency factor is only $\beta = 25\%$. Figure 6(a) shows how introducing a 20-nm SiO_x slot improves the coupling efficiency. The taller the waveguide the easier single-mode operation can be achieved over a wide range of widths. For $H = 500$ nm, a β -factor of 37% can be reached. The light coupled into the waveguide is entirely polarized along the z -direction ($\beta \approx \beta_z$), see Fig. 6(b). Simulations show that departing from the chosen slot height $H_g = 20$ nm does not change β significantly ($H_g \pm 10$ nm $\approx \beta \pm 4\%$). Fig. 6(c) shows the mode profiles of the supported TE and TM modes for $H = 220$ nm and $W = 350$ nm. Comparing with Fig. 2(b), we see that the TE-mode is not significantly modified by the slot, while the TM-mode shows an enhancement of the local field strength within the slot. The same local

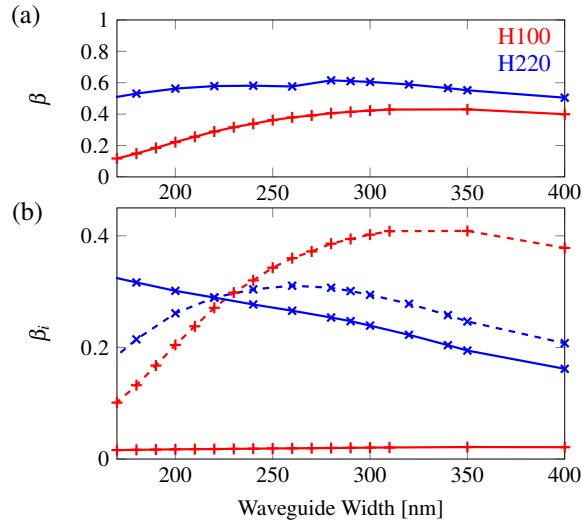


Fig. 5. Suspended SiN_x waveguide: a) Total coupling factor β to the guided modes as a function of the waveguide width W for two different waveguide heights $H = 100$ nm (red) and 220 nm (blue). b) Polarization dependent coupling factors β_y (dashed line) and β_z (plain line) as a function of the waveguide width W for two different waveguide heights $H = 100$ nm (red) and 220 nm (blue).

field enhancement is observed for tall waveguides ($H > W$) and is responsible for the improved coupling of the emitted photon to the single TM-mode, as discussed above.

The best coupling efficiencies in this study are obtained for suspended slot-waveguides, as in Fig. 1(d). Figure 7(a) displays the partial Purcell factors F_y (dashed lines), and F_z (plain lines) as a function of the waveguide width W for two waveguide heights: $H = 300$ nm (red line) and $H = 500$ nm (blue line). In striking contrast with the suspended waveguide without a slot (see Fig. 4(a)), the partial Purcell factor F_z now takes values significantly higher than one, ranging between 2.6 and 4.4 in the investigated range. Also notice that the partial Purcell factor F_y can be made much smaller than one when W approaches 100 nm. This shows that one can simultaneously enhance the spontaneous emission from a z -polarized dipole and inhibit the spontaneous emission from a y -polarized dipole. In that case, a highly polarized emission is expected in a TM-mode, despite the existence of a TE-mode. The simultaneous enhancement of F_z and reduction of F_y can be understood by looking at the mode profiles. Figure 7(b) shows that the slot enhances the strength of the TM modal field at the center of the waveguide where the emitter is positioned. The enhancement is stronger when there is no substrate under the waveguide since the modal area is smaller. It is responsible for the high values of F_z over the entire range of parameters. The reduced value of F_y is explained by the phenomenon already observed in Fig. 4(c). When the waveguide becomes thin enough in one particular dimension, the field of the mode polarized orthogonally to that direction is expelled from the centre of the waveguide, resulting in a reduced matter light coupling. Here, the TE-field is expelled from the waveguide when $W < 150$ nm, which results in a F_y -value significantly smaller than one.

Figure 8 displays the total coupling factor β and the partial coupling factors β_y and β_z for suspended slot-waveguides with height $H = 300$ nm (red lines) and $H = 500$ nm (blue lines). Figure 8(a) shows that, for both heights, the waveguide geometry leads to coupling factors as

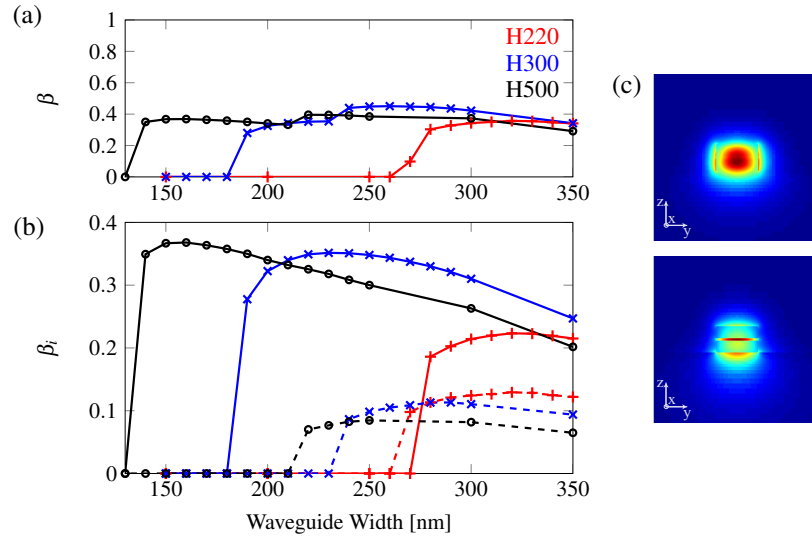


Fig. 6. SiN Slot waveguide on substrate: a) Total coupling factor β to the guided modes as a function of the waveguide width W for three different waveguide heights $H = 220$ nm (red), 300 nm (blue) and 500 nm (black). b) Polarization dependent coupling factors β_y (dashed line) and β_z (plain line) for the same waveguide dimensions as in a. The slot height is $H_g = 20$ nm. c) mode profiles of the two guided modes for a waveguide with $H = 220$ nm and $W = 350$ nm. Top: fundamental TE mode. Bottom: fundamental TM mode.

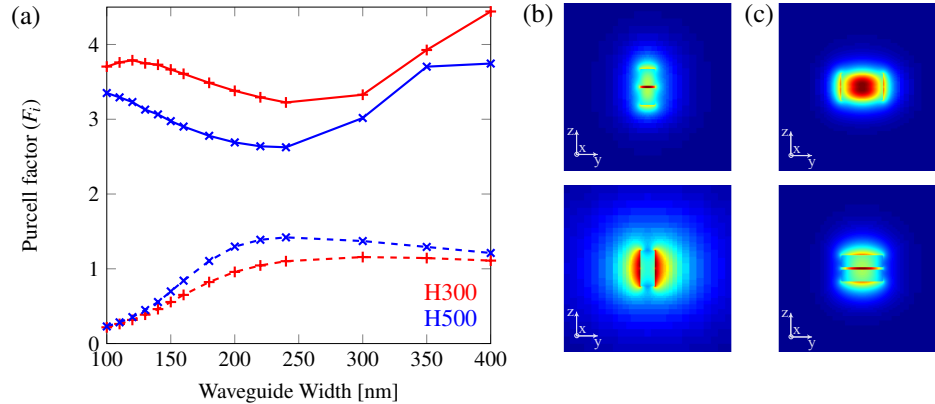


Fig. 7. Suspended SiN_x slot-waveguide: a) Partial Purcell factor F_y (dashed line), and F_z (plain line) as a function of the waveguide width W for two waveguide heights: $H=300$ nm (red line) and $H=500$ nm (blue line). b) Mode profiles of guided fundamental TE and TM modes for a waveguide with dimensions: b) $H = 220$ nm and $W = 350$ nm, c) $H = 300$ nm and $W = 130$ nm.

high as $\beta = 59\%$ when $W = 120$ nm. Figure 8(b) further shows that the β_z/β_y ratio is higher

in the $H = 300$ nm case than in the $H = 500$ nm case, in accordance with the discussion above and the Purcell factors displayed in Fig. 7(a). For $W = 120$ nm, β_x is negligible, $\beta_y = 3\%$, and $\beta_z = 56\%$. This results in a very high polarization ratio $\beta_z/\beta = 96\%$ for the guided light. Going to wider waveguides results in a higher β but also in a lower polarization ratio. A maximal overall coupling of 67% is found for a waveguide with dimension $H = 300$ nm and $W = 220$ nm, and $\beta_z/\beta = 74\%$. Replacing the SiO_x layer by an air slot, would result in even higher Purcell factors (F_z up to 14) and hence an even higher degree of polarization (98%) and total coupling (59%) can be achieved.

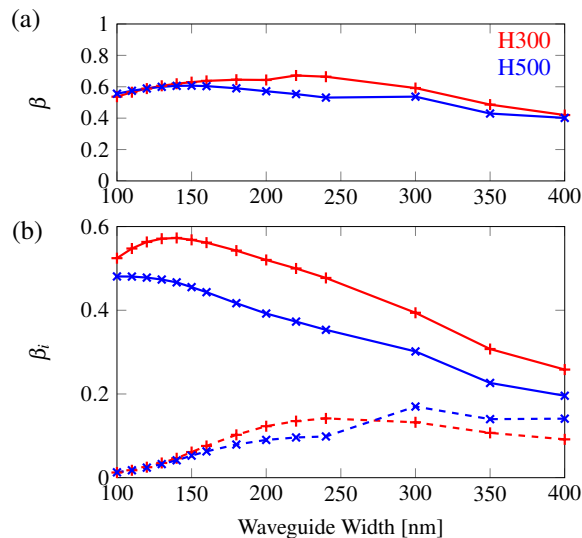


Fig. 8. Suspended SiN_x slot-waveguide: a) Total coupling factor β to the guided modes as a function of the waveguide width W for two different waveguide heights $H = 300$ nm (red) and 500 nm (blue). b) Polarization dependent coupling factors β_y (dashed line) and β_z (plain line) as a function of the waveguide width W for two different waveguide heights $H = 300$ nm (red) and 500 nm (blue).

Conclusions

Our study shows that high efficiency in-plane SP sources can in principal be realized using SiN_x photonic devices as simple as waveguides. We showed that light from a SP emitter can be efficiently coupled to the waveguide. High coupling factors β ranging between 40% and 67% were found in the four waveguide geometries under investigation. Furthermore, we showed that under certain geometrical conditions, the emitted photon can be coupled to a single polarized guided (TE or TM) mode. In that case, an effective polarized SP source is built even if the SP emitter itself is unpolarized. In suspended strip waveguides, we show that one can simultaneously achieve a good coupling factor $\beta = 43\%$ and a high polarization ratio $\beta_y/\beta=95\%$. In suspended slot waveguides, a higher coupling factor $\beta = 56\%$ is achievable in combination with a similar polarization ratio $\beta_z/\beta=96\%$.

These results demonstrate that high efficiency single-photon sources and complex optical circuits can be combined on a single photonic chip for quantum optics experiments. The SiN_x sources and optical circuits can be manufactured using well-established CMOS-compatible processing technology. Because the SiN_x transparency range extends from the visible to the

infrared, the envisaged platform is compatible with several types SP emitting inclusions such as colloidal quantum dots, nanoparticles containing a single color centre, and single-ion doped nanoparticles.

Acknowledgement

The authors acknowledge the Belgian Science Policy Office (IAP 7.35 photonics@be) and the Horizon2020 program (MSCA-ETN phonsi) for funding this research.